HEALTH AND MEDICINE

MUC5B mobilizes and MUC5AC spatially aligns mucociliary transport on human airway epithelium

Daniel Song[1], Ethan Iverson[2], Logan Kaler[3], Allison Boboltz[1], Margaret A. Scull[2]*, Gregg A. Duncan[1,3]*

Secreted mucus is a frontline defense against respiratory infection, enabling the capture and swift removal of infectious or irritating agents from the lungs. Airway mucus is composed of two mucins: mucin 5B (MUC5B) and 5AC (MUC5AC). Together, they form a hydrogel that can be actively transported by cilia along the airway surface. In chronic respiratory diseases, abnormal expression of these mucins is directly implicated in dysfunctional mucus clearance. Yet, the role of each mucin in supporting normal mucus transport remains unclear. Here, we generate human airway epithelial tissue cultures deficient in either MUC5B or MUC5AC to understand their individual contributions to mucus transport. We find that MUC5B and MUC5AC deficiency results in impaired and discoordinated mucociliary transport, respectively, demonstrating the importance of each mucin to airway clearance.

INTRODUCTION

Airway mucus is a complex biological fluid that shields the lungs from environmental insults through a process known as mucociliary clearance (MCC). In MCC, a mucus coating protects the underlying epithelium by acting as a physicochemical barrier that immobilizes inhaled pathogens and particulates (*1*, *2*). Unlike other mucosal tissues in the body, the airways can dynamically clear mucus—and trapped particulates—through shear forces exerted by the rapid beating of cilia on the epithelium (*3*, *4*). Normal MCC is essential for innate defense and is facilitated by a transportable mucus layer and coordinated ciliary activity (*5*). The primary secreted mucins expressed in the lungs are mucin 5B (MUC5B) and mucin 5AC (MUC5AC) (*6*, *7*). These mucins are large (megadalton range) glycoproteins with cysteine-rich domains at their N and C termini, which enable polymerization via disulfide bonds. Mucin biopolymers further arrange through physical entanglements forming a mucus gel stabilized by covalent and noncovalent interactions (*4*, *8*). The resulting hydrogel network acts as a solid-like barrier that controls the transport of nano- and microscale entities through physical and biochemical interactions while also having a liquid-like ability to flow in response to ciliary action (*9*–*13*). While MUC5B and MUC5AC are very similar in amino acid sequence and domain organization, recent evidence shows that they differ in assembly and N-terminal organization, with MUC5B mainly forming dimers and MUC5AC forming both dimers and higher-order oligomers (*14*, *15*). These subtle differences in macromolecular organization affect the functional properties of secreted mucins, such as effectiveness as a barrier and transportability, which have been studied in in vivo animal models (*16*). In Muc5ac/b knockout (KO) mice, Muc5b deficiency leads to impaired mucus transport and pathogen accumulation, while Muc5ac is shown to be dispensable for transport (*17*, *18*). Conversely, overexpression of Muc5b has been shown to cause mucociliary dysfunction, while overproduction of Muc5ac leads to protection against influenza virus infection (*19*, *20*).

In healthy lungs, MUC5B is the predominant mucin, while MUC5AC is expressed at lower levels (*6*, *7*); the ratio of MUC5B and MUC5AC is tightly regulated to ensure efficient MCC. However, in several chronic respiratory diseases, the production of MUC5AC increases because of type I and II immune responses, resulting in a mucus gel with abnormal mucin composition (*7*, *21*–*23*). Elevated MUC5AC in mucus has been identified as the major driver of MCC impairment and is correlated with enhanced viscoelastic properties, decreased lung function in chronic bronchitis, and mucus plugging in fatal asthma (*7*, *21*, *24*, *25*). How MUC5AC contributes to effective mucus clearance in healthy lung function, while driving the formation of stagnant mucus in disease, is unknown. As a result, there is growing interest in understanding how these two secreted mucins with similar domain structures—but varying functional properties—work in concert to enable efficient airway clearance. Moreover, the spatial coordination of transport on airway surfaces has been largely attributed to cilia organization and activity (*26*). However, the contribution of secreted mucins to tissue-scale alignment in MCC has not been widely considered.

In our studies, we developed in vitro airway epithelial systems deficient in one of the two gel-forming mucins to investigate the role and contribution of MUC5B and MUC5AC in MCC mechanisms. We used these in vitro human airway epithelial models to harvest MUC5B and MUC5AC gels for comparative assessment of their rheological properties. In addition, we measured mucociliary transport rates and flow orientation in real time. Our studies found that MUC5B deficiency leads to impaired mucus clearance, whereas MUC5AC deficiency leads to transport that lacks spatial coordination. Accordingly, we observed that supplementing MUC5B- and MUC5AC-deficient cultures with the absent mucin normalizes mucociliary transport. Together, our data demonstrate the functional significance of both mucins for promoting effective MCC and offers insight into the composition dependence of MCC impairment. This work also establishes the basis for therapeutic

[1]Fischell Department of Bioengineering, University of Maryland, College Park, MD 20742, USA. [2]Department of Cell Biology and Molecular Genetics, University of Maryland, College Park, MD 20742, USA. [3]Biophysics Program, University of Maryland, College Park, MD 20742, USA.
*Corresponding author. Email: gaduncan@umd.edu (G.A.D.); scull@umd.edu (M.A.S.)

interventions targeting mucin balance in the treatment of respiratory diseases.

RESULTS

Generation of MUC5B/AC-KO BCi-NS1.1 cultures

CRISPR-Cas9–mediated genome editing was used to generate in vitro human airway epithelial (HAE) models genetically deleted for one of the two gel-forming mucins. We designed two single-guide RNAs (sgRNAs) that target each mucin gene, *MUC5B* and *MUC5AC*, at different exons (table S1). Earlier exons were targeted to maximize KO efficiency, while two sgRNAs were designed to account for potential off-target effects. As our control, we used an sgRNA with no predicted target. The sgRNAs were cloned into a green fluorescent protein (GFP)–expressing lentiviral vector that also encodes the Cas9 nuclease. After lentivirus production, we transduced BCi-NS1.1 cells, an immortalized HAE basal cell line previously used for studies on mucin expression, and once differentiated, can be used for in vitro assessment of mucus clearance (*27*–*29*). Subsequently, transduced cells were expanded and sorted for GFP expression before differentiation (Fig. 1A). Using a T7 endonuclease cleavage assay, we confirmed editing at the correct genomic loci in undifferentiated cells, evidenced by heteroduplex fragments in all KO conditions (fig. S1, A and B). To verify that lentiviral transduction did not affect normal differentiation of BCi-NS1.1 cultures, we measured the transepithelial electrical resistance (TEER) 28 days into the air-liquid interface (ALI) culture and confirmed TEER values that were within reported ranges in all conditions, indicative of cell polarization and differentiation into a pseudostratified epithelium (Fig. 1B) (*30*). To evaluate intracellular mucin expression in HAE cultures, we performed en face immunostaining, which revealed expression of both MUC5B and MUC5AC in control cultures, MUC5AC expression in MUC5B KO cultures, and MUC5B expression in MUC5AC KO cultures (Fig. 1C). Because MUC5B and MUC5AC are secreted extracellularly as high–molecular weight cross-linked polymers, we also performed Western blot analysis on reduced mucus samples collected from apical washes of cultures. Results confirmed the loss of MUC5B and MUC5AC expression in KO cultures using respective sgRNAs (Fig. 1D). Agarose gel–based Western blot analysis of unreduced (full-length) secreted mucins and measured disulfide bond concentrations also showed that MUC5B KO and MUC5AC KO did not disrupt mucin assembly into high–molecular weight glycoproteins (fig. S2). Collectively, these data confirm that mucus secretions from MUC5B-KO cultures are primarily composed of MUC5AC, while secretions from MUC5AC-KO cultures are composed of MUC5B, allowing us to study the properties of hydrogels composed of each secreted airway mucin.

Viscoelasticity of MUC5B and MUC5AC gels

To evaluate the biophysical properties of gels composed of either MUC5B or MUC5AC, we performed macro- and microrheology on pooled mucus samples collected from control and KO cultures. Using macrorheology, we observed elastic-dominant properties for all mucus samples ($G' > G''$) indicative of a cross-linked polymer network. We also established that the samples exhibited rheological properties in range of previously reported values for mucus collected in vitro and ex vivo (Fig. 2A and fig. S3) (*11*–*13*). While MUC5AC gels resulted in slightly higher mean complex viscosities than other gel types, these differences were not statistically significant (Fig. 2B). We next measured percent solids concentration of each sample, since the biophysical properties of polymer gels are highly sensitive to changes in solids concentration. We found that the solids concentration of pooled mucus samples was within a physiological range (2 to 4%) (Fig. 2C) (*4*, *11*). Using a previously reported fluorometric assay to detect O-linked glycoproteins (*10*), we estimated that ~50% of total solids consists of mucin in samples tested (fig. S4). While macrorheological properties have major implications in flow and transport, the microstructural network of mucus is important to its function as a barrier to inhaled material (Fig. 2D) (*4*). Therefore, we used particle tracking microrheology (PTM) to assess diffusion of mucoinert nanoparticles (MIPs) through mucus with different compositions to probe mucus microstructure. Results showed that MUC5AC gels had significantly reduced MIP diffusion, as measured by mean square displacement (MSD) (Fig. 2E). These data are indicative of reduced pore size in MUC5AC gels compared to MUC5B gels and mucus collected from control cultures (Fig. 2F). Furthermore, we found that the network structure of MUC5B gels is similar in nature to mucus obtained from control cultures, whereas MUC5AC gels possessed a significantly tighter and heterogeneous structure (Fig. 2, G to J). We also found that there were no significant differences in macro- and microrheology measurements of MUC5B and MUC5AC gels harvested from cultures with equivalent KO condition (KO1 and KO2) but that were targeted using different sgRNAs.

MUC5B-KO cultures exhibit reduced mucociliary transport and MUC5AC-KO cultures exhibit discoordinated transport

We next examined the mucociliary transport rates of mucus produced from MUC5B-KO or MUC5AC-KO cultures to investigate the contribution of each gel-forming mucin to MCC. To do so, we deposited 2-μm microspheres onto KO cultures and tracked the movement of particles in real time (Fig. 3A). We observed that the movement of microspheres on MUC5B-KO cultures was significantly reduced compared to the nontargeted control cultures. While functional transport was maintained in MUC5AC-KO cultures, we observed a loss of unidirectional flow (Fig. 3B). Quantification of microsphere speed confirmed that MUC5B-KO cultures had significantly reduced transport rates compared to control and MUC5AC-KO cultures (Fig. 3C). We next quantified the directionality of mucus flow on the control and MUC5AC-KO cultures. The overall directionality of mucus flow ($\theta_{average}$) was quantified by averaging all measured angular directions of individual microsphere trajectories (θ_i) (Fig. 3D). We found that control cultures resulted in an overall alignment of flow direction, where 94% of the microspheres moved within 10° to −10° of overall flow (Fig. 3E). However, MUC5AC-KO cultures resulted in an irregular flow pattern that resembled circular swirls, where only 35 to 50% of microspheres aligned with the average flow direction (Fig. 3, F and G). These differences in mucus flow transport rate and directionality were not likely the result of changes in the periciliary layer properties since we confirmed normal cilia beat frequency and normal cilia expression, as demonstrated in % tubulin-positive area (Fig. 3, H to J, and fig. S5). Further, we find that mucociliary transport is normal in both KO cultures supplemented with mucus harvested from control cultures (fig. S6, A and B). This suggests that ciliary activity and coordination of the epithelium are unaffected in our KO cultures.

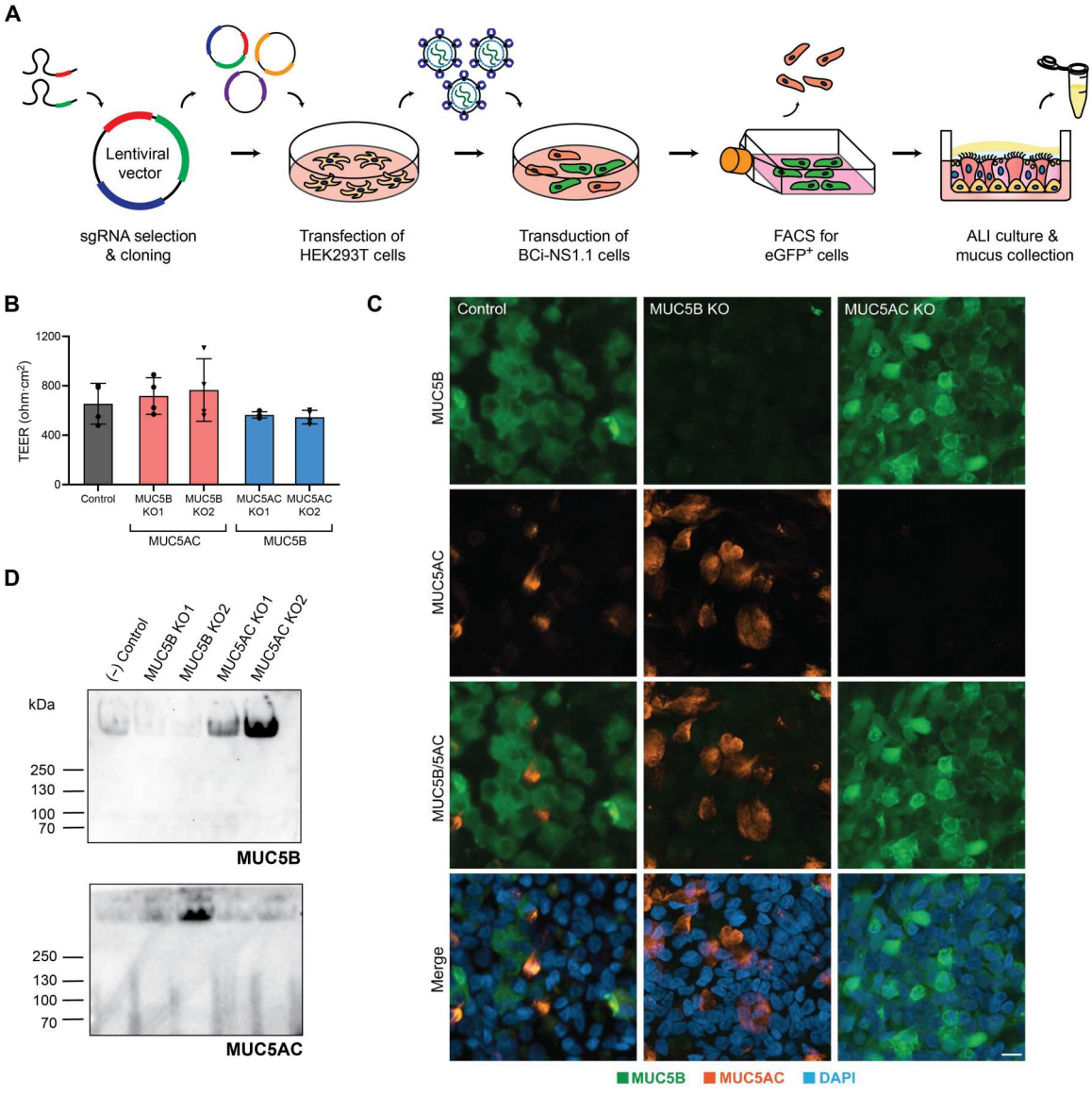

Fig. 1. Generation and validation of MUC5B/AC-KO cultures. (**A**) Overview of the MUC5B/MUC5AC gene-targeting approach via lentivirus-mediated delivery of sgRNA and CRISPR-Cas9. Transduced and sorted cells were differentiated at air-liquid interface (ALI). Once fully differentiated, the mucus gel was collected by apically washing cultures. HEK293T, human embryonic kidney–293T; FACS, fluorescence-activated cell sorting; EGFP, green fluorescent protein. (**B**) TEER measurements in fully differentiated MUC5B/MUC5AC KO cultures. KO1 corresponds to BCi-NS1.1 cells transduced with sgRNA1, and KO2 corresponds to cells transduced with sgRNA2. ($n = 4$ biological replicates). No statistically significant differences between groups as assessed by one-way analysis of variance (ANOVA). (**C**) Immunofluorescence staining for MUC5B (green) and MUC5AC (orange) in MUC5B/AC-KO cultures. Nuclei were stained with 4′,6-diamidino-2-phenylindole (DAPI) (blue). Representative two-dimensional (2D) projections from *z*-stack images for each secreted mucin are shown. Cultures were washed with 10 mM dithiothreitol before fixing and staining for intracellular mucins. Scale bar, 10 μm. (**D**) Western blot analysis of mucus gels collected from apical washes of fully differentiated control and KO cultures. Samples were separated by electrophoresis (4 to 20% tris-glycine gel, reducing conditions) and detected by immunoblot for MUC5B and MUC5AC.

Transplanting exogenous mucus rescues impaired clearance

On the basis of our previous data, which demonstrate abnormal transport with the loss of one of the two mucins, we hypothesized that supplementing KO cultures with the absent mucin could restore stalled and/or irregular mucociliary transport phenotypes. To test this, we transplanted 20 μl of exogenous MUC5B and MUC5AC gels onto KO cultures and tracked the movement of microspheres on the cultures (Fig. 4A). We chose MUC5B-KO1 and MUC5AC-KO2 as representative cultures for transplantation experiments. We found that transplantation of MUC5B onto MUC5B-KO cultures resulted in a significant increase in transport rates, as well as unidirectional flow (Fig. 4, B to D). However, transplantation of MUC5AC gels onto their native MUC5B-KO cultures did not result in a significant change in transport rate. The addition of either MUC5B or MUC5AC gels onto MUC5AC-KO cultures did not result in any significant change to transport rates (Fig. 4E) but did improve directionality, where ~85% of the microspheres

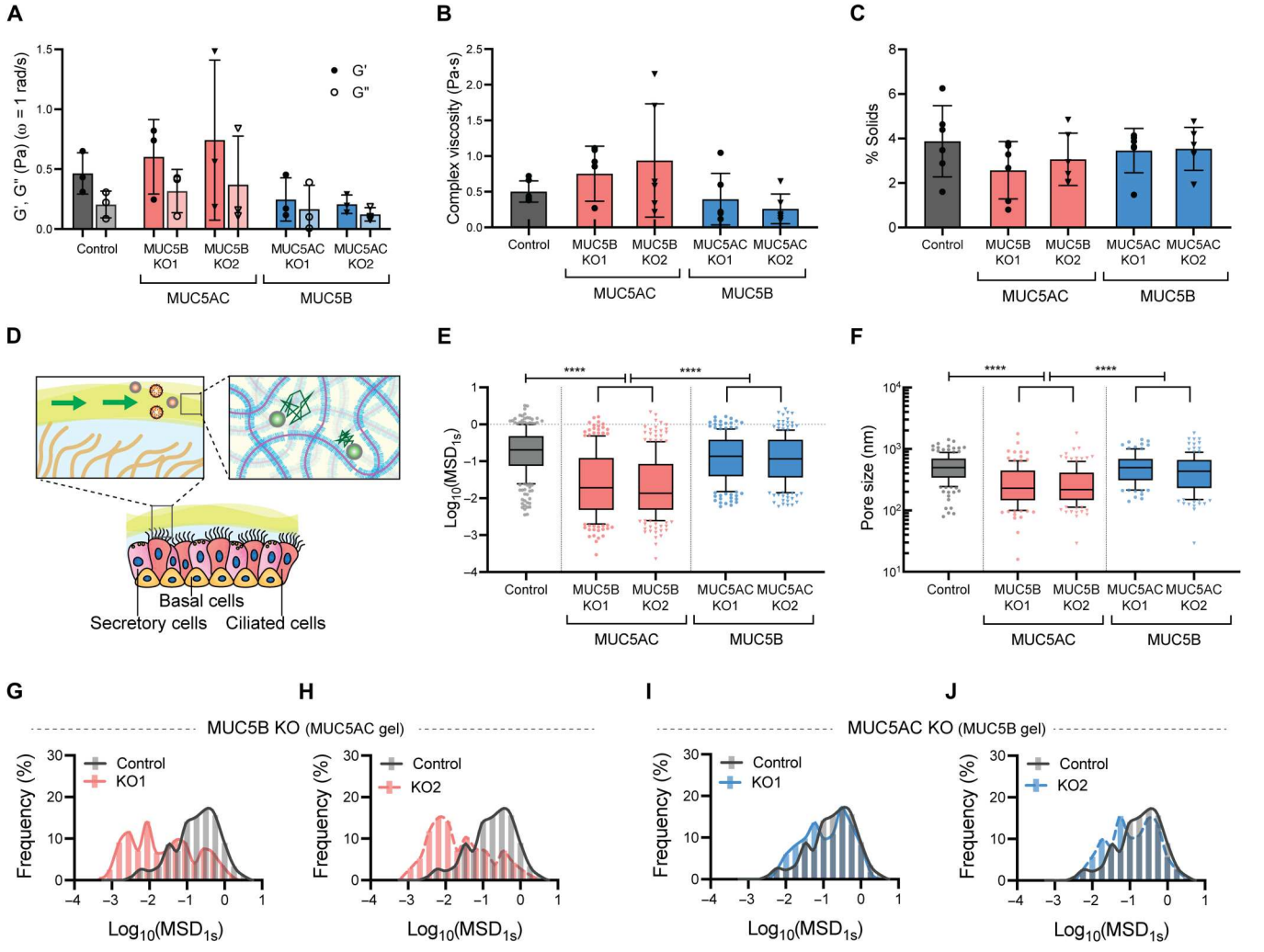

Fig. 2. Viscoelastic properties of mucus produced from MUC5B/AC-KO cultures. (**A**) Elastic and viscous moduli (G′ and G″) at ω = 1 rad/s measured using macrorheology. Moduli show G′-dominant behavior, indicative of a viscoelastic gel. (**B**) Complex viscosity measured using macrorheology. (**C**) Solids concentration (%, w/v) in pooled mucus samples from MUC5B/AC-KO and control cultures. (A to C) Individual data points represent each independent measurement. (**D**) Airway mucus acts as a vehicle for pathogen clearance, providing the lungs with a robust defense mechanism. Mucus also has a microstructural network that can immobilize diffusing particles. (**E**) Diffusion of 100-nm polyethylene glycol (PEG)–coated nanoparticles (PEG-NP) in mucus samples from KO cultures as measured by $\log_{10}$ MSD at time lag of 1 s (MSD_{1s}). Whiskers are drawn down to the 5th percentile, up to the 95th percentile, and the outliers are shown as individual points. (**F**) Estimated pore sizes of mucus samples. (**G** to **J**) Frequency distribution of $\log_{10}(MSD_{1s})$ for 100 nm PEG-NP diffusion in mucus harvested from control cultures compared to (G) MUC5B-KO1, (H) MUC5B-KO2, (I) MUC5AC-KO1, and (J) MUC5AC-KO2 cultures. (n = 3 biological replicates). Significance was determined by one-way ANOVA (A to C) and Kruskal-Wallis test with Dunn's correction (E and F). ****$P < 0.0001$.

are directionally aligned with overall flow with their flow angles falling within 10° to −10° of average flow direction (Fig. 4, F and G). To evaluate the impact of supplemental gel volume on transport dynamics in KO cultures, we repeated these experiments using only 5 μl of exogenous MUC5B and MUC5AC (fig. S6, C to F). We found that transplantation of MUC5B or MUC5AC at a reduced volume of 5 μl did not result in fully recovered transport in MUC5B KO cultures (fig. S6, C and D). However, supplementation of MUC5AC KO cultures with 5 μl of MUC5AC led to improved flow alignment, whereas the flow remained poorly aligned in cultures supplemented with 5 μl of MUC5B (fig. S6, E and F).

DISCUSSION

In these studies, we established in vitro HAE models that are genetically depleted of one of the two gel-forming mucins to understand their role and overall contribution to airway mucus clearance. We targeted *MUC5B* and *MUC5AC* genes in the BCi-NS1.1 human airway basal cell line and demonstrated successful editing in undifferentiated cultures. MUC5B and MUC5AC KO was further confirmed in cells and in pooled mucus washings after differentiation. MUC5B-KO cultures produced gels composed primarily of MUC5AC, while MUC5AC-KO cultures produced MUC5B gels, which allowed us to study each mucin independently. We note that our Western blot analysis indicated that KO cultures produced slightly elevated levels of respective mucins compared to

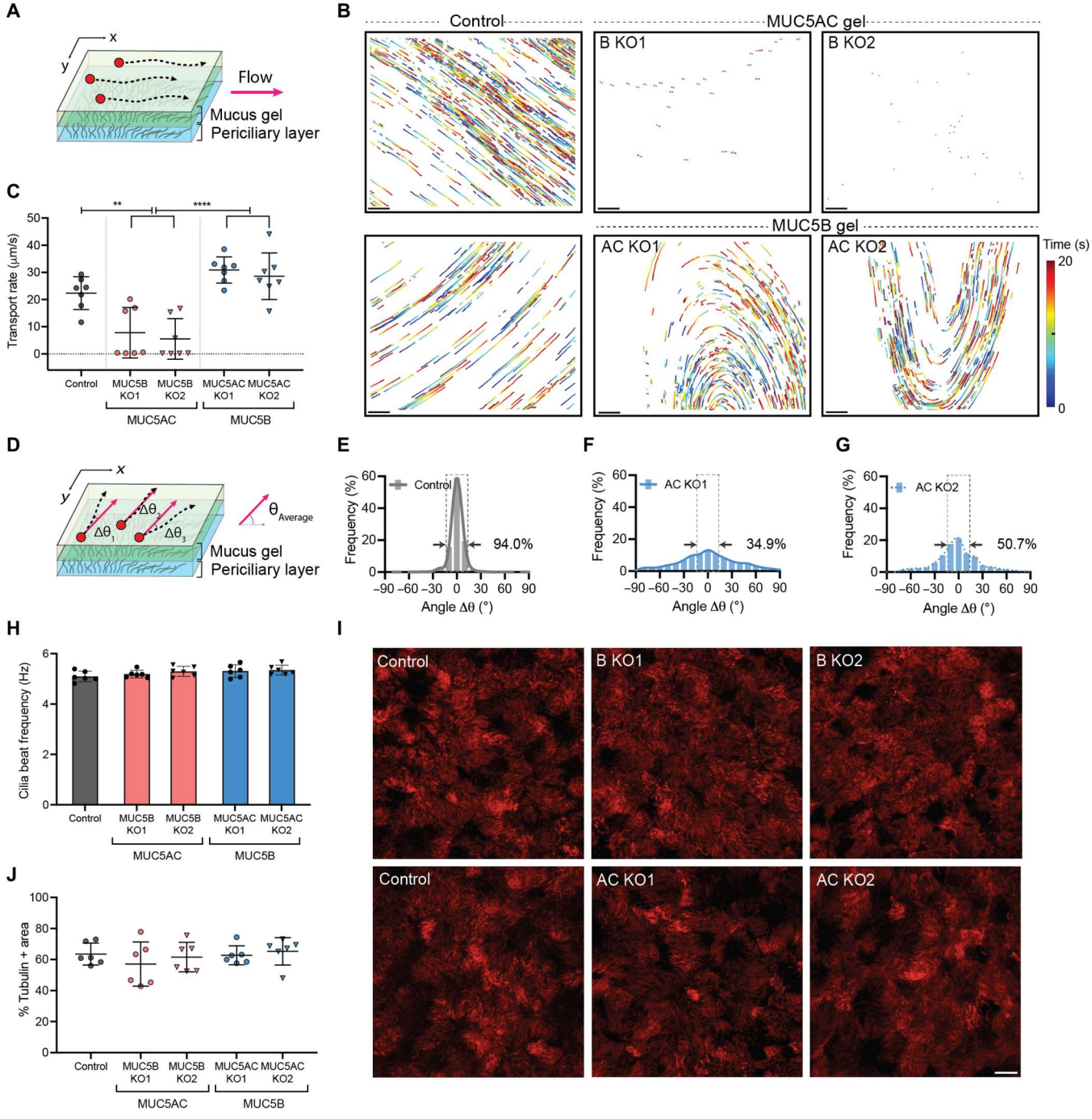

Fig. 3. MCC dynamics of MUC5B/AC-KO cultures. (**A**) Mucociliary transport rate is measured by apically applying 2-μm microspheres to fully differentiated cultures and measuring particle displacement over time. (**B**) Images of microsphere trajectories over time. Trajectories show 20 s of motion with a color scale that indicates elapsed time. Scale bar, 100 μm. (**C**) Mucociliary transport rates of MUC5B/AC-KO cultures. (**D**) Alignment in microsphere trajectory angle was calculated as $\Delta\theta = \theta_{Average} - \theta_i$, where $\theta_{Average}$ is the average flow direction and θ_i is individual microsphere trajectory angle. (**E** to **G**) Frequency distribution of $\Delta\theta$ in (E) control, (F) MUC5AC-KO1, and (G) MUC5AC-KO2 cultures. Percentages refer to percent of particles falling within 10° to −10° of $\Delta\theta$, which is indicated by the arrows. Transport rates and directionality were determined from 7 cultures ($n = 7$). Individual data points represent median transport rate of microspheres determined from three fields per culture. (**H**) Cilia beat frequencies of MUC5B/AC KO cultures. Beat frequency was determined from six cultures ($n = 6$). Individual data points represent average beat frequency determined from nine fields per culture. (**I**) Immunofluorescence staining for acetylated α-tubulin in MUC5B/AC-KO cultures. Micrographs show 2D projections of acquired z-stack images. Scale bar, 10 μm. (**J**) Quantification of +tubulin % area. Significance was determined by one-way ANOVA (C, H, and J). $^{**}P < 0.05$ and $^{****}P < 0.0001$.

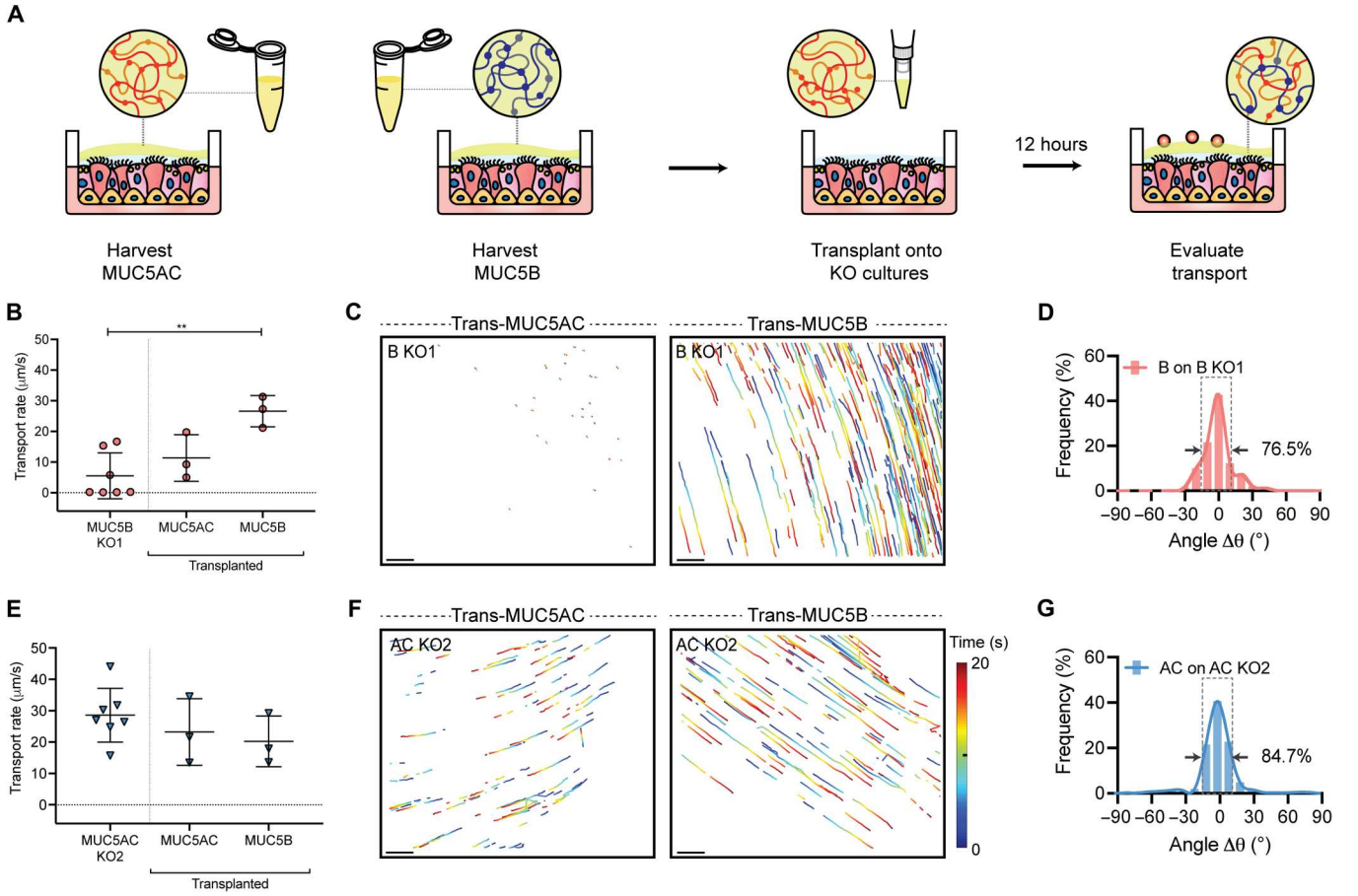

Fig. 4. MCC dynamics after MUC5B and MUC5AC supplementation in KO cultures. (**A**) Exogenous mucus collected from KO cultures was transplanted onto fully differentiated KO cultures to supplement with additional and/or absent MUC5B/AC. After transplantation, cultures were incubated for 12 hours to allow equilibration. (**B**) Mucociliary transport rates after transplanting MUC5AC and MUC5B on MUC5B-KO1 culture. Transport rates of transplanted mucus were determined from three cultures ($n = 3$). (**C**) Images of microsphere trajectories on MUC5B-KO1 cultures with transplanted mucus. Scale bar, 100 μm. (**D**) Frequency distribution of Δθ on MUC5B-KO1 cultures supplemented with MUC5B. (**E**) Mucociliary transport rates after transplanting MUC5AC and MUC5B on MUC5AC-KO2 cultures. (**F**) Images of microsphere trajectories on MUC5AC-KO2 cultures with transplanted mucus. Scale bars, 100 μm. (**G**) Frequency distribution of Δθ on MUC5AC-KO2 cultures supplemented with MUC5AC. (C and F) Trajectories show 20 s of motion with a color scale that indicates elapsed time. Individual data points represent median transport rate of microspheres determined from three fields per culture. Percentages refer to percent of particles falling within 10° to −10° of Δθ, which is indicated by the arrows. Significance was determined by one-way ANOVA (B and E). $^{**}P < 0.05$.

control cultures, while overall percent solids and protein concentration were conserved. These results may indicate that MUC5B and MUC5AC secretion is hydrodynamically controlled, regardless of mucin type. The pathways that regulate secretion of each mucin after KO should be explored in future studies. In addition, MUC5B and MUC5AC KO may influence production of other mucus-associated proteins (*31*), which should also be further explored in subsequent experiments.

Using our KO cultures, we assessed the biophysical properties of mucus samples with different mucin composition. Our results indicate that gels composed of MUC5AC have altered microstructural properties compared to MUC5B gels, where pore size is significantly reduced and heterogeneous. These results are consistent with recent findings that show that MUC5AC forms a tighter network with high degrees of branching, while MUC5B organizes in linear strands (*15*). The smaller pore size in MUC5AC gels have implications for their functional role as a protective gel against pathological and chemical insults to the airway. In previous studies, MUC5AC has been shown to protect against viral respiratory pathogens such as influenza virus and to prevent parasite infiltration (*20*, *23*, *32*). We also observed major differences in transportability of gels composed of different mucin types. MUC5AC gels produced from MUC5B-KO cultures were poorly cleared, while MUC5B gels from MUC5AC-KO cultures were more easily transported. These data are consistent with previous mouse models that showed Muc5b-KO, but not Muc5ac-KO, resulted in impaired MCC and mucus accumulation in the airways (*17*). In humans, recent evidence has shown that congenital absence of MUC5B results in impaired mucus clearance (*33*). This may be due, in part, to macromolecular organization of mucins, where MUC5B forms linear gels that can be easily transported via ciliary activity, while MUC5AC forms a tighter gel, which increases friction at the mucus-periciliary layer interface, resulting in poor clearance (*3*, *15*). While bulk rheological properties are known to affect transport properties of mucus gels, our data showed no resolvable differences in viscosities between gels composed of different mucin types.

We note that previous studies have predicted MUC5AC to form more elastic gels than MUC5B (*15*). We also found that the solids concentration of MUC5AC gels was slightly reduced in comparison to MUC5B gels. Given the strong dependence of mucus viscoelasticity on solids concentration (*4*), we expect that MUC5B and MUC5AC gels with a matched solids concentration would have greater differences in their viscoelastic properties.

Despite functional transport of MUC5B gels on MUC5AC-KO cultures, we observed that MUC5AC deficiency led to poor directionality with local swirls, while control cultures that expressed both mucins showed global order. These transport patterns have been previously observed in HAE in vitro models and attributed to hydrodynamic active coupling between mucus and cilia, where changes in mucus properties and cilia density can alter the overall orientation of mucus flow (*34*, *35*). While the role of MUC5AC in mucociliary transport has been largely overlooked, our data suggest that MUC5AC-enhanced mucus viscoelasticity plays a significant role in hydrodynamic coupling between the mucus and periciliary layers, driving long-range transport and effective clearance. This can also be explained by our transplantation experiments with exogenous mucus, where we demonstrated that supplementation of KO cultures with the absent mucin can rescue and improve irregular transport phenotypes. We note that supplementation with high volumes (20 μl) of MUC5B to MUC5B-expressing cultures also improved transport coordination—likely by increasing mucin concentration and mucus gel viscoelasticity—leading to enhanced hydrodynamic coupling. However, at lower volumes (5 μl), only the addition of MUC5AC to MUC5B-expressing cultures led to culture-wide alignment in mucociliary transport. Together, these experiments demonstrate the biological importance of both gel-forming mucins, MUC5B and MUC5AC, for efficient airway mucus transport.

The current understanding of impaired mucus clearance has primarily focused on the imbalance in osmotic pressure between the mucus and periciliary layers, the result of a dehydrated or hyperconcentrated mucus gel that is not easily cleared (*3*, *36*). However, our findings shed light on the mechanisms of defective MCC dictated by mucus composition, independent of concentration. While increased MUC5AC may contribute to protection against inhaled pathogens, disproportionate increases have been associated with pathogenesis of chronic obstructive lung diseases and airway obstruction (*7*, *21*). Mucus plugs from individuals with fatal asthma also show MUC5AC enrichment where physical tethering of MUC5AC to the epithelium disrupts normal transport function. This is in accordance with our data, which show that the secretion of MUC5AC alone absent of MUC5B leads to severe impairment in MCC. However, we have yet to determine the relative contribution of MUC5AC adhesion and tethering to the epithelium toward the impaired transport observed in our MUC5B KO cultures. Another limitation of this study is the use of an in vitro model, which by nature does not include submucosal glands (SMGs), which are important contributors to mucin production and functional airway clearance (*37*, *38*). Future studies in MUC5B- and MUC5AC-deficient animal models, ideally in a larger animal with extensive SMG development in the airways (e.g., pigs), to explore these potential effects in vivo are certainly warranted.

In conclusion, our study provides unique insight into the contribution of each gel-forming mucin—MUC5B and MUC5AC—to MCC mechanisms. Our findings suggest that secretion of MUC5B and MUC5AC offer a means for the airway epithelium to dynamically control mucus transport velocity and flow alignment. While MUC5AC has been considered a potential therapeutic target for asthma (*17*, *18*), we predict that preserving baseline levels of MUC5AC could be important in maintaining flow orientation to facilitate effective removal of pathogens. To resolve MUC5AC-induced MCC dysfunction, ongoing work on mucolytic strategies that target the disulfide bonds in mucus gels for normalizing clearance may prove useful, as MUC5AC-enriched gels are likely to be more extensively cross-linked (*15*, *39*). This work also establishes the premise for future development of new precision therapies aimed at restoring an optimal balance of MUC5B and MUC5AC secretion in airway diseases.

MATERIALS AND METHODS

CRISPR-Cas9–mediated KO of MUC5B and MUC5AC

We used lentivirus for CRISPR-Cas9–mediated gene targeting of MUC5B and MUC5AC in BCi-NS1.1 cells, a human telomerase reverse transcriptase (h-TERT) immortalized human airway basal cell line, provided by. R. Crystal, which their group established and characterized in previous work (*27*). Two sgRNAs that target different regions of MUC5B and MUC5AC were selected on the basis of favorable targeting using the Doench and Xu scores. To generate negative control, we designed sgRNA sequences with no matching sequence in the genome (nontargeting control). Selected gRNAs were cloned into a GFP-expressing lentiviral vector, pLENTICRISPRv2-GFP [a gift from F. Zhang (Addgene, plasmid no. 52961; http://n2t.net/addgene:52961; RRID:Addgene_52961)], which also encodes Cas9 nuclease. Lentiviral stocks were generated by cotransfecting plentiCRISPRv2, pCMV-VSV-G [a gift from B. Weinberg [Addgene, plasmid no., 8454; http://n2t.net/addgene:8454; RRID:Addgene_8454], and psPAX2 [a gift from D. Trono (Addgene, plasmid no., 12260; http://n2t.net/addgene:12260; RRID:Addgene_12260)] into human embryonic kidney–293T cells with jetPrime (Polyplus) in cell culture media, Dulbecco′s modified Eagle′s medium (Gibco) supplemented with 10% fetal bovine serum, using the manufacturer′s protocol. BCi-NS1.1 cells were transduced at 40 to 60% confluence using harvested lentiviruses in media with a final concentration of 20 mM Hepes (Gibco) and Polybrene (4 μg/ml; AmericanBio). BCi-NS1.1 cells were then centrifuged (1000*g* for 1 hour at 37°C) and incubated at 37°C overnight. At 60 to 80% confluence cells were passaged, expanded, and sorted for enhanced GFP (eGFP) expression.

T7 endonuclease cleavage assay

DNA from transduced, sorted (eGFP$^+$) cells was extracted using QuickExtract DNA Extraction Solution (Lucigen). The EnGen Mutation Detection Kit (New England Biolabs) was used for amplification of target DNA, heteroduplex formation, and heteroduplex digestion, using the manufacturer′s protocol. Final DNA products were separated and visualized in a 1% agarose gel through gel electrophoresis.

Cell culture

Transduced and sorted (eGFP$^+$) BCi-NS1.1 cells were seeded on plastic at ~3000 cells/cm^2 in PneumaCult-Ex Plus media (STEMCELL Technologies) and incubated at 37°C, 5% CO_2. Once cells reached 70 to 80% confluency, they were dissociated using 0.05%

trypsin EDTA for 5 min at 37°C. To establish well-differentiated HAE tissue cultures grown at ALI, BCi-NS1.1 cells were seeded on 12-mm diameter transwell inserts (Corning Costar) coated with type 1 collagen (50 μg/ml) from rat tail (Corning) at ~10,000 cells/cm^2. Expansion media, PneumaCult-Ex Plus, was used to feed cells in both the apical and basolateral compartments until 100% confluency. After reaching confluency, the apical media was removed to transition from submerged to ALI culture, and the basolateral media was replaced with PneumaCult-ALI (STEMCELL Technologies). All cells were grown for 28 days to reach differentiation with media exchanged every other day. TEER was quantified in cultures using the Millicell Electrical Resistance System ERS-2 Volt-Ohm Meter (Millipore).

Mucus collection

Once fully differentiated, mucus was allowed to accumulate before collection every 3 to 4 days. Mucus samples were harvested by washing apical compartments with phosphate-buffered saline (PBS) for 30 min at 37°C. After 30 min of incubation, the solution of mucus and PBS was collected (*11*, *13*). Samples were loaded into Amicon Ultra 100-kDa filters (MilliporeSigma) and centrifuged at 14,000*g* for 20 min to remove excess PBS for mucin isolation. Mucus samples were stored at −80°C for long-term storage (> 2 weeks) or stored at 4°C (*28*). Collected samples were pooled for Western blot analysis, solids concentration analysis, biophysical characterization, and transport experiments.

Immunostaining for secreted mucins and cilia

Fully differentiated control and KO cultures were washed with PBS three times and fixed using 4% paraformaldehyde for 30 min at room temperature. For immunostaining of mucins, cultures were washed with 10 mM 1,4-dithiothreitol (DTT) for 10 min before fixation. After fixation, inserts were washed with PBS and blocked with 5% bovine serum albumin (BSA) in PBS and 0.01% Triton X-100 for 1 hour at room temperature. After blocking, fixed cultures were incubated overnight at 4°C with primary antibodies or Alexa Fluor–conjugated antibodies in 5% BSA in PBS. The antibodies that were used were mouse anti-MU5AC (1:500; catalog no. ab3649, Abcam) and rabbit anti-MUC5B UNC414 (1:500; gifted by C. Ehre), anti-acetylated α-tubulin Alexa Fluor 647 (cilia marker, clone 6-11B-1, sc23950, Santa Cruz Biotechnology; 1:2000), and ZO-1 monoclonal antibody Alexa Fluor 488 (tight junction marker, ZO1-1A12, Invitrogen; 1:2000). Secondary antibodies used were donkey anti-mouse immunoglobulin G (IgG) (H + L) Highly Cross-Adsorbed Secondary Antibody, Alexa Fluor 555 (Thermo Fisher Scientific, A-21202, RRID AB_141607), and goat anti-rabbit IgG (H + L) secondary antibody, fluorescein isothiocyanate (Novus, NB7159). Inserts were washed with PBS three times and imaged using a 63× objective (Zeiss C-Apochromat, 1.2 numerical aperture, water immersion) on a Zeiss 800 LSM microscope (Zeiss). Representative images are *z*-stack. Quantification of % tubulin-positive area was performed in Fiji using the automated thresholding function.

Western blot analysis

Pooled mucus samples were used for Western blot analysis. Protein concentration of samples was quantified using bicinchoninic acid assay (Pierce, Thermo Fisher Scientific). SDS–polyacrylamide gel electrophoresis–based Western blot analysis for MUC5B and MUC5AC was performed under reducing conditions by adapting previously reported methods (*40*, *41*). First, equal amounts of mucus samples (10 μg) were mixed with NuPAGE Sample Reducing Agent (10×) (Novex, Invitrogen) and SDS sample buffer (2×) (Novex, Invitrogen) and loaded into each lane and run on a 4 to 20% tris-glycine gel (Novex, Invitrogen). Proteins were transferred to a polyvinylidene fluoride (PVDF) membrane (GE Healthcare) and blocked with 5% (w/v) fat-free milk protein in tris-buffered saline, 0.1% Tween (TBS-T) at room temperature before staining with primary antibodies. Agarose-based Western blot analysis under nonreducing conditions was conducted as previously described (*42*, *43*). First, equal amounts of mucus samples (10 μg) were mixed with 1× loading buffer (40 mM tris-acetate, 1 mM EDTA buffer, 1% SDS, 50% glycerol, and 0.002% bromophenol blue) and loaded into each lane of a 0.8% agarose gel (0.1% SDS). Proteins were separated by electrophoresis at 12 V overnight (or 16 hours). Samples were then vacuum-transferred from the agarose gel to a PVDF membrane in 4× SSC buffer (0.6 M sodium chloride and 0.06 M sodium citrate) and blocked with 5% (w/v) fat-free milk protein in TBS-T at room temperature. Primary antibody incubation was overnight at 4°C in 5% (w/v) fat-free milk protein. The primary antibodies that were used were mouse anti-MU5AC (1:1000; catalog no. ab3649, Abcam) and rabbit anti-MUC5B UNC414 (1:1000), provided by C. Ehre. After washing in TBS-T, membranes were probed with secondary antibodies for 1 hour at room temperature in blocking buffer. The secondary antibodies that were used were anti-mouse IgGk–horseradish peroxidase (HRP) (sc-516102, Santa Cruz Biotechnology; 1:10,000) and anti-rabbit HRP (32460, Invitrogen; 1:10,000). Imaging was performed with a chemiluminescent SuperSignal Dura reagent (Thermo Fisher Scientific) on an iBright 1500 (Thermo Fisher Scientific).

Total solids, mucin, and disulfide bond concentration

We measured solids concentrations of mucus samples by aliquoting 50 μl of mucus on weighing paper of known mass and recording the combined mass of the mucus sample and paper. The samples were then placed on a heat plate at 60°C for 4 to 5 hours. The final mass of the dried sample and weighing paper was recorded and used to calculate percentage of solids concentration. Mucin concentrations of mucus samples were determined by reaction of 2-cyanoacetamide (CNA) and O-linked glycans as previously described (*10*). Mucus samples were diluted 20-fold and homogenized by vortexing. CNA reagent was prepared by mixing 200 μl of 0.6 M CNA with 1 ml of 0.15 M NaOH. Fifty microliters of mucus suspension was mixed with 60 μl of CNA reagent and incubated at 100°C for 30 min. After incubation, 0.5 ml of 0.6 M borate buffer (pH 8.0) was added to quench reaction. Fluorescence intensity was measured at excitation and emission wavelength of 340 and 420 nm, respectively. Mucin concentrations were calculated by comparing the fluorescence intensity reading to a standard curve generated using known concentration of mucin from bovine submaxillary gland (Sigma-Aldrich). Mucin–to–total solids ratio was determined by dividing mucin concentration with solids concentration. The concentration of disulfide bonds was quantified as previously described (*10*). Briefly, mucus samples were resuspended in 8 M guanidine-HCl to a final volume to 500 μl (473 μl of guanidine-HCl per sample). Samples were then treated with 10% (v/v) 500 mM iodoacetamide at room temperature for 1 hour before treatment with 10% (v/v) 1 M DTT at 37°C for 2 hours. The samples were passed through 7-kDa molecular weight cutoff Zebra desalting columns

to remove small molecules and buffer exchange into 50 mM tris-HCl (pH 8.0). Standards were made from serial dilution of 5 mM L-cysteine. For each sample and standard, equal volume was combined with 2 mM monobromobimane in a 96-well black plate and incubated at room temperature for 15 min. The plate was read at 395-nm excitation and 490-nm emission.

Bulk rheology

Dynamic rheological measurements of mucus gels harvested and pooled from ALI cultures were performed using the ARES G2 rheometer (TA Instruments) with a 40-mm-diameter 2° cone and plate geometry at 25°C. To determine the linear viscoelastic region of the fully formed gel, a strain sweep measurement was collected from 0.1 to 10% strain at a frequency of 1 rad s^{-1}. To determine the elastic modulus, $G'(\omega)$, and viscous modulus, $G''(\omega)$, a frequency sweep measurement was conducted within the linear viscoelastic region of the gel, at 1% strain amplitude and angular frequencies from 0.1 to 10 rad s^{-1}. For each condition (control, MUC5B KO, and MUC5AC KO), three replicate samples were analyzed.

Particle tracking microrheology

Carboxylate-modified, fluorescent polystyrene (PS) nanoparticles (PS–COOH; Life Technologies) with a diameter of 100 nm were coated with a high surface density of polyethylene glycol (PEG) via a carboxyl-amine linkage using 5-kDa methoxy PEG-amine (Creative PEGWorks) as previously reported (*9*, *44*). Particle size and zeta potential were measured in 10 mM NaCl at pH 7 using a NanoBrook Omni (Brookhaven Instruments). We measured diameters of 122 nm and zeta potentials of −0.54 ± 1.16 for 100-nm PEG-coated PS nanoparticles, respectively. The diffusion of the PEG-coated nanoparticles (PEG-NP) in mucus gels was measured using fluorescence video microscopy. Twenty-five microliters of mucus was added to the chamber along with 1 μl of ~0.002% (w/v) suspension of PEG-NP 30 min before PTM experiments. Videos were collected using a Zeiss 800 LSM microscope with a 63× water-immersion objective and an Axiocam 702 camera (Zeiss) at a frame rate of 33 Hz for 10 s at room temperature. For each condition, three independent samples were analyzed, and for each biological replicate, at least three high-speed videos were recorded. The particle tracking analysis was performed using a previously developed image processing algorithm (*44*, *45*). MSD as a function of time lag (τ) was calculated as

$$\langle \Delta r^2(\tau) \rangle = \langle (x^2 + y^2) \rangle \quad (1)$$

for each particle. Using the generalized Stokes-Einstein relation, measured MSD values were used to compute viscoelastic properties of the hydrogels. The Laplace transform of $\langle \Delta r^2(\tau) \rangle$, $\langle \Delta r^2(s) \rangle$, is related to viscoelastic spectrum $\tilde{G}(s)$ using the equation

$$\tilde{G}(s) = 2k_B T / [\pi a s \langle \Delta r^2(s) \rangle] \quad (2)$$

where $k_B T$ is the thermal energy, a is the particle radius, and s is the complex Laplace frequency. The complex modulus can be calculated as

$$G^*(\omega) = G'(\omega) + G''(i\omega) \quad (3)$$

with $i\omega$ being substituted for s, where i is a complex number and ω is frequency. Hydrogel network pore size, ξ, is estimated on the basis of G' using the equation

$$\xi \approx (k_B T / G')^{1/3} \quad (4)$$

Mucociliary transport and ciliary beat frequency

For measurement of mucociliary transport rate, a 4-μl suspension of 2-μm red fluorescent PS microspheres (Sigma-Aldrich; 1:1000 dilution in PBS) was apically applied to native mucus, which was allowed to accumulate for 1 to 2 days before analysis. Cultures were washed before applying the suspension of microspheres to remove accumulated mucus layer. After equilibration overnight, videos of the three regions were recorded at ×10 magnification using a Zeiss 800 LSM microscope. Images were collected at a frame rate of 0.5 Hz for 20 s on the plane of the mucus gel. The microsphere tracking data analysis is based on an image processing algorithm that was custom-written in MATLAB (*28*, *46*). Briefly, the analysis software computes the *xy*-plane trajectories of each fluorescent microsphere in each frame. Using the trajectory data, displacement of microspheres was computed, and the transport rate was calculated by dividing the distance traveled by total elapsed time. Directionality of mucus flow was determined by measuring the angular direction of individual microsphere trajectories (θ_i), where i refers to microsphere number and computing the average angle ($\theta_{Average}$).

$$\theta_{Average} = \frac{1}{n}\sum_{i=1}^{n}\theta_i \quad (5)$$

Coordination of mucus flow was assessed by determining $\Delta\theta$, calculated as $\Delta\theta = \theta_{Average} - \theta_i$ and comparing the frequency distributions of $\Delta\theta$ in control and MUC5AC-KO conditions. To measure ciliary beat frequency, 10-s videos at a frame rate of 20 Hz were recorded at ×20 magnification in ≥3 randomly selected regions of each BCi-NS1.1 culture using bright field. Using a custom-written algorithm in MATLAB, the number of local pixel intensity maxima was counted, which indicates beating of cilia. Beat frequency was determined by dividing the number of beats over the total elapsed time. All measurements described were repeated in at least six cultures per condition tested, and all cultures were age-matched on the basis of the number of days since transitioning into ALI.

Mucus transplantation

Reconstituted mucus samples from KO culture washings were used for transplantation studies. Five and 20 μl of mucus were applied to the apical surface of ALI cultures that had been washed with PBS for 30 min (*28*, *47*). Two-micrometer red fluorescent PS microspheres were applied immediately after transplantation of exogenous mucus. Mucociliary transport rates were measured after equilibration overnight as described in the methods above.

Statistical analysis

All graphing and statistical analyses were performed using GraphPad Prism 8 (GraphPad Software). For comparisons between groups, one-way analysis of variance (ANOVA), followed by a Tukey post hoc correction was performed. Kruskal-Wallis with Dunn's correction was used for comparison of multiple groups with non-Gaussian distributions. Bar graphs show mean and SD, and box-and-whiskers plots show median. Differences were considered statistically different at the level of $P < 0.05$.

Supplementary Materials

This PDF file includes:
Table S1
Figs. S1 to S6

Other Supplementary Material for this manuscript includes the following:
Movies S1 to S5

View/request a protocol for this paper from *Bio-protocol*.

REFERENCES AND NOTES

1. J. V. Fahy, B. F. Dickey, Airway mucus function and dysfunction. *N. Engl. J. Med.* **363**, 2233–2247 (2010).
2. M. Kesimer, C. Ehre, K. A. Burns, C. W. Davis, J. K. Sheehan, R. J. Pickles, Molecular organization of the mucins and glycocalyx underlying mucus transport over mucosal surfaces of the airways. *Mucosal Immunol.* **6**, 379–392 (2013).
3. B. Button, L.-H. Cai, C. Ehre, M. Kesimer, D. B. Hill, J. K. Sheehan, R. C. Boucher, M. Rubinstein, A periciliary brush promotes the lung health by separating the mucus layer from airway epithelia. *Science* **337**, 937–941 (2012).
4. D. Song, D. Cahn, G. A. Duncan, Mucin biopolymers and their barrier function at airway surfaces. *Langmuir* **36**, 12773–12783 (2020).
5. M.-K. Khelloufi, E. Loiseau, M. Jaeger, N. Molinari, P. Chanez, D. Gras, A. Viallat, Spatio-temporal organization of cilia drives multiscale mucus swirls in model human bronchial epithelium. *Sci. Rep.* **8**, 2447 (2018).
6. M. E. Lachowicz-Scroggins, S. Yuan, S. C. Kerr, E. M. Dunican, M. Yu, S. D. Carrington, J. V. Fahy, Abnormalities in MUC5AC and MUC5B protein in airway mucus in asthma. *Am. J. Respir. Crit. Care Med.* **194**, 1296–1299 (2016).
7. M. Kesimer, A. A. Ford, A. Ceppe, G. Radicioni, R. Cao, C. W. Davis, C. M. Doerschuk, N. E. Alexis, W. H. Anderson, A. G. Henderson, R. G. Barr, E. R. Bleecker, S. A. Christenson, C. B. Cooper, M. K. Han, N. N. Hansel, A. T. Hastie, E. A. Hoffman, R. E. Kanner, F. Martinez, R. Paine III, P. G. Woodruff, W. K. O'Neal, R. C. Boucher, Airway mucin concentration as a marker of chronic bronchitis. *N. Engl. J. Med.* **377**, 911–922 (2017).
8. D. J. Thornton, K. Rousseau, M. A. McGuckin, Structure and function of the polymeric mucins in airways mucus. *Annu. Rev. Physiol.* **70**, 459–486 (2008).
9. B. S. Schuster, J. S. Suk, G. F. Woodworth, J. Hanes, Nanoparticle diffusion in respiratory mucus from humans without lung disease. *Biomaterials* **34**, 3439–3446 (2013).
10. G. A. Duncan, J. Jung, A. Joseph, A. L. Thaxton, N. E. West, M. P. Boyle, J. Hanes, J. S. Suk, Microstructural alterations of sputum in cystic fibrosis lung disease. *JCI Insight* **1**, e88198 (2016).
11. D. B. Hill, P. A. Vasquez, J. Mellnik, S. A. McKinley, A. Vose, F. Mu, A. G. Henderson, S. H. Donaldson, N. E. Alexis, R. C. Boucher, M. G. Forest, A biophysical basis for mucus solids concentration as a candidate biomarker for airways disease. *PLOS ONE* **9**, e87681 (2014).
12. A. L. Innes, S. D. Carrington, D. J. Thornton, S. Kirkham, K. Rousseau, R. H. Dougherty, W. W. Raymond, G. H. Caughey, S. J. Muller, J. V. Fahy, Ex vivo sputum analysis reveals impairment of protease-dependent mucus degradation by plasma proteins in acute asthma. *Am. J. Respir. Crit. Care Med.* **180**, 203–210 (2009).
13. M. R. Markovetz, D. B. Subramani, W. J. Kissner, C. B. Morrison, I. C. Garbarine, A. Ghio, K. A. Ramsey, H. Arora, P. Kumar, D. B. Nix, T. Kumagai, T. M. Krunkosky, D. C. Krause, G. Radicioni, N. E. Alexis, M. Kesimer, M. Tiemeyer, R. C. Boucher, C. Ehre, D. B. Hill, Endotracheal tube mucus as a source of airway mucus for rheological study. *Am. J. Physiol. Lung Cell. Mol. Physiol.* **317**, L498–L509 (2019).
14. L. Bonser, D. Erle, Airway mucus and asthma: The role of MUC5AC and MUC5B. *J. Clin. Med.* **6**, 112 (2017).
15. J. Carpenter, Y. Wang, R. Gupta, Y. Li, P. Haridass, D. B. Subramani, B. Reidel, L. Morton, C. Ridley, W. K. O'Neal, M.-P. Buisine, C. Ehre, D. J. Thornton, M. Kesimer, Assembly and organization of the N-terminal region of mucin MUC5AC: Indications for structural and functional distinction from MUC5B. *Proc. Natl. Acad. Sci. U.S.A.* **118**, e2104490118 (2021).
16. C. E. Wagner, K. M. Wheeler, K. Ribbeck, Mucins and their role in shaping the functions of mucus barriers. *Annu. Rev. Cell Dev. Biol.* **34**, 189–215 (2018).
17. M. G. Roy, A. Livraghi-Butrico, A. A. Fletcher, M. M. McElwee, S. E. Evans, R. M. Boerner, S. N. Alexander, L. K. Bellinghausen, A. S. Song, Y. M. Petrova, M. J. Tuvim, R. Adachi, I. Romo, A. S. Bordt, M. G. Bowden, J. H. Sisson, P. G. Woodruff, D. J. Thornton, K. Rousseau, M. M. De La Garza, S. J. Moghaddam, H. Karmouty-Quintana, M. R. Blackburn, S. M. Drouin, C. W. Davis, K. A. Terrell, B. R. Grubb, W. K. O'Neal, S. C. Flores, A. Cota-Gomez, C. A. Lozupone, J. M. Donnelly, A. M. Watson, C. E. Hennessy, R. C. Keith, I. V. Yang, L. Barthel, P. M. Henson, W. J. Janssen, D. A. Schwartz, R. C. Boucher, B. F. Dickey, C. M. Evans, Muc5b is required for airway defence. *Nature* **505**, 412–416 (2014).
18. C. M. Evans, D. S. Raclawska, F. Ttofali, D. R. Liptzin, A. A. Fletcher, D. N. Harper, M. A. McGing, M. M. McElwee, O. W. Williams, E. Sanchez, M. G. Roy, K. N. Kindrachuk, T. A. Wynn, H. K. Eltzschig, M. R. Blackburn, M. J. Tuvim, W. J. Janssen, D. A. Schwartz, B. F. Dickey, The polymeric mucin Muc5ac is required for allergic airway hyperreactivity. *Nat. Commun.* **6**, 6281 (2015).
19. L. A. Hancock, C. E. Hennessy, G. M. Solomon, E. Dobrinskikh, A. Estrella, N. Hara, D. B. Hill, W. J. Kissner, M. R. Markovetz, D. E. Grove Villalon, M. E. Voss, G. J. Tearney, K. S. Carroll, Y. Shi, M. I. Schwarz, W. R. Thelin, S. M. Rowe, I. V. Yang, C. M. Evans, D. A. Schwartz, Muc5b overexpression causes mucociliary dysfunction and enhances lung fibrosis in mice. *Nat. Commun.* **9**, 5363 (2018).
20. C. Ehre, E. N. Worthington, R. M. Liesman, B. R. Grubb, D. Barbier, W. K. O'Neal, J. M. Sallenave, R. J. Pickles, R. C. Boucher, Overexpressing mouse model demonstrates the protective role of Muc5ac in the lungs. *Proc. Natl. Acad. Sci. U.S.A.* **109**, 16528–16533 (2012).
21. L. R. Bonser, L. Zlock, W. Finkbeiner, D. J. Erle, Epithelial tethering of MUC5AC-rich mucus impairs mucociliary transport in asthma. *J. Clin. Invest.* **126**, 2367–2371 (2016).
22. E. Doz, N. Noulin, E. Boichot, I. Guénon, L. Fick, M. Le Bert, V. Lagente, B. Ryffel, B. Schnyder, V. F. J. Quesniaux, I. Couillin, Cigarette smoke-induced pulmonary inflammation is TLR4/MyD88 and IL-1R1/MyD88 signaling dependent. *J. Immunol.* **180**, 1169–1178 (2008).
23. D. Rajan, E. L. O'Keefe, C. Travers, C. McCracken, S. Geoghegan, M. T. Caballero, P. L. Acosta, F. Polack, L. J. Anderson, MUC5AC levels associated with respiratory syncytial virus disease severity. *Clin. Infect. Dis.* **67**, 1441–1444 (2018).
24. E. M. Dunican, B. M. Elicker, D. S. Gierada, S. K. Nagle, M. L. Schiebler, J. D. Newell, W. W. Raymond, M. E. Lachowicz-Scroggins, S. Di Maio, E. A. Hoffman, M. Castro, S. B. Fain, N. N. Jarjour, E. Israel, B. D. Levy, S. C. Erzurum, S. E. Wenzel, D. A. Meyers, E. R. Bleecker, B. R. Phillips, D. T. Mauger, E. D. Gordon, P. G. Woodruff, M. C. Peters, J. V. Fahy; National Heart Lung and Blood Institute (NHLBI) Severe Asthma Research Program (SARP), Mucus plugs in patients with asthma linked to eosinophilia and airflow obstruction. *J. Clin. Invest.* **128**, 997–1009 (2018).
25. D. S. Raclawska, F. Ttofali, A. A. Fletcher, D. N. Harper, B. S. Bochner, W. J. Janssen, C. M. Evans, Mucins and their sugars. Critical mediators of hyperreactivity and inflammation. *Ann. Am. Thorac. Soc.* **13** (Suppl. 1), S98–S99 (2016).
26. G. R. Ramirez-San Juan, A. J. T. M. Mathijssen, M. He, L. Jan, W. Marshall, M. Prakash, Multi-scale spatial heterogeneity enhances particle clearance in airway ciliary arrays. *Nat. Phys.* **16**, 958–964 (2020).
27. M. S. Walters, K. Gomi, B. Ashbridge, M. A. S. Moore, V. Arbelaez, J. Heldrich, B.-S. Ding, S. Rafii, M. R. Staudt, R. G. Crystal, Generation of a human airway epithelium derived basal cell line with multipotent differentiation capacity. *Respir. Res.* **14**, 135 (2013).
28. D. Song, E. Iverson, L. Kaler, S. Bader, M. A. Scull, G. A. Duncan, Modeling airway dysfunction in asthma using synthetic mucus biomaterials. *ACS Biomater Sci. Eng.* **7**, 2723–2733 (2021).
29. A. T. Reid, K. S. Nichol, P. C. Veerati, F. Moheimani, A. Kicic, S. M. Stick, N. W. Bartlett, C. L. Grainge, P. A. B. Wark, P. M. Hansbro, D. A. Knight, Blocking notch3 signaling abolishes MUC5AC production in airway epithelial cells from individuals with asthma. *Am. J. Respir. Cell Mol. Biol.* **62**, 513–523 (2020).
30. H. W. Chu, C. Rios, C. Huang, A. Wesolowska-Andersen, E. G. Burchard, B. P. O'Connor, T. E. Fingerlin, D. Nichols, S. D. Reynolds, M. A. Seibold, CRISPR-Cas9-mediated gene knockout in primary human airway epithelial cells reveals a proinflammatory role for MUC18. *Gene Ther.* **22**, 822–829 (2015).
31. G. Radicioni, R. Cao, J. Carpenter, A. A. Ford, T. T. Wang, Y. Li, M. Kesimer, The innate immune properties of airway mucosal surfaces are regulated by dynamic interactions between mucins and interacting proteins: The mucin interactome. *Mucosal Immunol.* **9**, 1442–1454 (2016).
32. S. Z. Hasnain, C. M. Evans, M. Roy, A. L. Gallagher, K. N. Kindrachuk, L. Barron, B. F. Dickey, M. S. Wilson, T. A. Wynn, R. K. Grencis, D. J. Thornton, Muc5ac: A critical component mediating the rejection of enteric nematodes. *J. Exp. Med.* **208**, 893–900 (2011).
33. G. Costain, Z. Liu, V. Mennella, G. Radicioni, A. N. Goczi, A. Albulescu, S. Walker, B. Ngan, D. Manson, R. Vali, M. Khan, N. Palaniyar, D. B. Hill, D. A. Hall, C. R. Marshall, M. Knowles, M. A. Zariwala, M. Kesimer, S. D. Dell, Hereditary mucin deficiency caused by biallelic loss of function of *MUC5B*. *Am. J. Respir. Crit. Care Med.* **205**, 761–768 (2022).
34. S. Gsell, E. Loiseau, U. D'Ortona, A. Viallat, J. Favier, Hydrodynamic model of directional ciliary-beat organization in human airways. *Sci. Rep.* **10**, 8405 (2020).
35. E. Loiseau, S. Gsell, A. Nommick, C. Jomard, D. Gras, P. Chanez, U. D'Ortona, L. Kodjabachian, J. Favier, A. Viallat, Active mucus–cilia hydrodynamic coupling drives self-organization of human bronchial epithelium. *Nat. Phys.* **16**, 1158–1164 (2020).
36. W. H. Anderson, R. D. Coakley, B. Button, A. G. Henderson, K. L. Zeman, N. E. Alexis, D. B. Peden, E. R. Lazarowski, C. W. Davis, S. Bailey, F. Fuller, M. Almond, B. Qaqish, E. Bordonali, M. Rubinstein, W. D. Bennett, M. Kesimer, R. C. Boucher, The relationship of mucus concentration (hydration) to mucus osmotic pressure and transport in chronic bronchitis. *Am. J. Respir. Crit. Care Med.* **192**, 182–190 (2015).

37. L. S. Ostedgaard, M. P. Price, K. M. Whitworth, M. H. A. Alaiwa, A. J. Fischer, A. Warrier, M. Samuel, L. D. Spate, P. D. Allen, B. M. Hilkin, G. S. R. Ibarra, M. E. O. Bezara, B. J. Goodell, S. E. Mather, L. S. Powers, M. R. Stroik, N. D. Gansemer, C. E. Hippee, K. Zarei, J. A. Goeken, T. R. Businga, E. A. Hoffman, D. K. Meyerholz, R. S. Prather, D. A. Stoltz, M. J. Welsh, Lack of airway submucosal glands impairs respiratory host defenses. *eLife* **9**, e59653 (2020).
38. A. J. Fischer, M. I. Pino-Argumedo, B. M. Hilkin, C. R. Shanrock, N. D. Gansemer, A. L. Chaly, K. Zarei, P. D. Allen, L. S. Ostedgaard, E. A. Hoffman, D. A. Stoltz, M. J. Welsh, M. H. Abou Alaiwa, Mucus strands from submucosal glands initiate mucociliary transport of large particles. *JCI Insight* **4**, e124863 (2019).
39. C. Ehre, Z. L. Rushton, B. Wang, L. N. Hothem, C. B. Morrison, N. C. Fontana, M. R. Markovetz, M. F. Delion, T. Kato, D. Villalon, W. R. Thelin, C. R. Esther Jr., D. B. Hill, B. R. Grubb, A. Livraghi-Butrico, S. H. Donaldson, R. C. Boucher, An improved inhaled mucolytic to treat airway muco-obstructive diseases. *Am. J. Respir. Crit. Care Med.* **199**, 171–180 (2019).
40. A. Ermund, L. N. Meiss, A. M. Rodriguez-Pineiro, A. Bähr, H. E. Nilsson, S. Trillo-Muyo, C. Ridley, D. J. Thornton, J. J. Wine, H. Hebert, N. Klymiuk, G. C. Hansson, The normal trachea is cleaned by MUC5B mucin bundles from the submucosal glands coated with the MUC5AC mucin. *Biochem. Biophys. Res. Commun.* **492**, 331–337 (2017).
41. E. Iverson, K. Griswold, D. Song, T. B. Gagliardi, K. Hamidzadeh, M. Kesimer, S. Sinha, M. Perry, G. A. Duncan, M. A. Scull, Membrane-tethered mucin 1 is stimulated by interferon and virus infection in multiple cell types and inhibits influenza a virus infection in human airway epithelium. *MBio* **13**, e0105522 (2022).
42. K. A. Ramsey, Z. L. Rushton, C. Ehre, Mucin agarose gel electrophoresis: Western blotting for high-molecular-weight glycoproteins. *J. Vis. Exp.* **2016**, e54153 (2016).
43. D. Preciado, S. Goyal, M. Rahimi, A. M. Watson, K. J. Brown, Y. Hathout, M. C. Rose, MUC5B is the predominant mucin glycoprotein in chronic otitis media fluid. *Pediatr. Res.* **68**, 231–236 (2010).
44. K. Joyner, D. Song, R. F. Hawkins, R. D. Silcott, G. A. Duncan, A rational approach to form disulfide linked mucin hydrogels. *Soft Matter* **15**, 9632–9639 (2019).
45. B. S. Schuster, L. M. Ensign, D. B. Allan, J. S. Suk, J. Hanes, Particle tracking in drug and gene delivery research: State-of-the-art applications and methods. *Adv. Drug Deliv. Rev.* **91**, 70–91 (2015).
46. T. B. Gagliardi, M. E. Goldstein, D. Song, K. M. Gray, J. W. Jung, M. A. Ignacio, K. M. Stroka, G. A. Duncan, M. A. Scull, Rhinovirus C replication is associated with the endoplasmic reticulum and triggers cytopathic effects in an in vitro model of human airway epithelium. *PLOS Pathog.* **18**, e1010159 (2022).
47. M. Woodall, B. Reidel, M. Kesimer, R. Tarran, D. L. Baines, Culture with apically applied healthy or disease sputum alters the airway surface liquid proteome and ion transport across human bronchial epithelial cells. *Am. J. Physiol. Cell Physiol.* **321**, C954–C963 (2021).

Acknowledgments: We acknowledge the BioWorkshop core facility in the Fischell Department of Bioengineering at the University of Maryland–College Park for use of their dynamic light scattering instrument, microplate reader, and rheometer and the MPRI Flow Cytometry and Cell Sorting Facility. We acknowledge support and guidance from D. Preciado and Y. Chen (Children's National Hospital) on agarose-based Western blot analysis of MUC5B and MUC5AC. **Funding:** This work was supported by the Burroughs Wellcome Fund Career Award at the Scientific Interface (to G.A.D.), the Cystic Fibrosis Foundation grant DUNCAN18I0 (to G.A.D. and M.A.S.), the National Institutes of Health grant R21AI142050 (to M.A.S. and G.A.D.), the National Institutes of Health grant R01HL151840 (to M.A.S.), the National Institutes of Health grant R01HL160540 (to G.A.D.), and the National Institutes of Health grant T32AI125186A (to E.I. and L.K.). **Author contributions:** Conceptualization: D.S., M.A.S., and G.A.D. Methodology: D.S., E.I., L.K., A.B., M.A.S., and G.A.D. Investigation: D.S., E.I., L.K., and A.B. Visualization: D.S., L.K., and A.B. Supervision: M.A.S. and G.A.D. Writing—original draft: D.S. Writing—review and editing: D.S., E.I., M.A.S., and G.A.D. **Competing interests:** The authors declare that they have no competing interests. **Data and materials availability:** All data needed to evaluate the conclusions in the paper are present in the paper and/or the Supplementary Materials. The CRISPR-Cas9–modified BCi-NS1.1 cells used in this work may be provided by G.A.D. and M.A.S. pending scientific review and a completed material transfer agreement. Requests for the modified BCi-NS1.1 cells should be submitted to gaduncan@umd.edu and scull@umd.edu.

Submitted 12 April 2022
Accepted 27 October 2022
Published 25 November 2022
10.1126/sciadv.abq5049